STEM CELLS TRANSLATIONAL MEDICINE®

TISSUE-SPECIFIC PROGENITOR AND STEM CELLS

# Targeting p38 Mitogen-Activated Protein Kinase Signaling Restores Subventricular Zone Neural Stem Cells and Corrects Neuromotor Deficits in *Atm* Knockout Mouse

JEESUN KIM, PAUL K.Y. WONG

**Key Words.** ATM • Neural stem cells • p38 • Oxidative stress • Purkinje cells

Department of Molecular Carcinogenesis, University of Texas M.D. Anderson Cancer Center, Smithville, Texas, USA

Correspondence: Paul K.Y. Wong, Ph.D., University of Texas M.D. Anderson Cancer Center, 1808 Park Road 1C, Smithville, Texas 78957, USA. Telephone: 512-237-9456; Fax: 512-237-2444; e-mail: pkwong@mdanderson.org

Received December 19, 2011; accepted for publication May 31, 2012; first published online in SCTM *EXPRESS* ■■■.


1066-5099/2012/$20.00/0

http://dx.doi.org/10.5966/sctm.2011-0063

## ABSTRACT

**Ataxia-telangiectasia (A-T) is a progressive degenerative disorder that results in major neurological disability. In A-T patients, necropsy has revealed atrophy of cerebellar cortical layers along with Purkinje and granular cell loss. We have previously identified an oxidative stress-mediated increase in phospho-p38 mitogen-activated protein kinase (MAPK) and the resultant downregulation of Bmi-1 and upregulation of p21 as key components of the mechanism causing defective proliferation of neural stem cells (NSCs) isolated from the subventricular zone (SVZ) of *Atm*$^{-/-}$ mice. However, the in vivo aspect of alteration in SVZ tissue and the functional significance of p38MAPK activation in NSCs for neuropathogenesis of ATM deficiency remain unknown. Here we show that the NSC population was abnormally decreased in the SVZ of 3-month-old *Atm*$^{-/-}$ mice; this decrease was accompanied by p38MAPK activation. However, after a 2-month treatment with the p38MAPK inhibitor SB203580, starting at 1 month old, *Atm*$^{-/-}$ mice showed restoration of normal levels of Bmi-1 and p21 with the rescue of NSC population in the SVZ. In addition, treated *Atm*$^{-/-}$ mice exhibited more Purkinje cells in the cerebellum. Most importantly, motor coordination of *Atm*$^{-/-}$ mice was significantly improved in the treatment group. Our results show for the first time in vivo evidence of depleted NSCs in the SVZ of *Atm*$^{-/-}$ mice and also demonstrate that pharmacologic inhibition of p38MAPK signaling has the potential to treat neurological defects of A-T. This study provides a promising approach targeting the oxidative stress-dependent p38 signaling pathway not only for A-T but also for other neurodegenerative disorders.** STEM CELLS TRANSLATIONAL MEDICINE *2012; 1:000–000*

## INTRODUCTION

Ataxia-telangiectasia (A-T) is primarily a progressive neurodegenerative disease, in which the *Atm* (A-T mutated) gene is mutated. Symptoms of A-T typically manifest within the first few years of life, when children exhibit ataxia. Progression of the disease is relentless and usually fatal. The mechanisms underlying A-T disease are still incompletely understood, and there is currently no cure [1]. A key function of the ATM protein is to sense and regulate cellular redox status using a complex network of downstream signaling pathways. In utero, ATM function is not required because the embryo is protected. When a newborn is exposed to oxygen and environmental stress ATM is activated to maintain cellular redox homeostasis. In ATM deficiency, cellular redox homeostasis is severely disrupted, resulting in abnormally high levels of reactive oxygen species (ROS). With age, increasing ROS accumulation leads to progressive neurodegeneration [2]. This offers an explanation for why ATM deficiency does not have overt neuropathological effects during embryonic development, and the sign of neurodegenerative symptoms gradually progresses after birth.

The predominant neurological abnormalities in A-T are primarily characterized by the loss of cerebellar Purkinje cells (PCs) [1–4]. With time, however, other regions, such as dopaminergic neurons in the substantia nigra of the brain, are also affected. In *Atm*$^{-/-}$ mice, moderate to severe levels of degeneration of PCs in the cerebellum have been reported [5–11]. Study by others using another ATM-deficient mouse model found abnormal PCs in older *Atm*$^{-/-}$ mice [9]. This phenotype is similar to recent observations in the PCs in the cerebellar tissue from an A-T patient [4]. In addition, Atm-null mice have movement coordination defects that are consistent with cerebellar dysfunction [10–13]. Together, these findings establish that some neuropathological abnormalities seen in A-T patients are present in *Atm*$^{-/-}$ mice, indicating that these mice are a useful model by which to study

A-T neurodegeneration. Therefore, we have used $Atm^{-/-}$ mice to identify potential targets that contribute to the neuropathology and motor coordination deficits of A-T and to develop therapeutic treatments for A-T.

During postnatal neurogenesis, ATM expression is abundant in proliferating neural stem cells (NSCs) but is markedly reduced as the cells differentiate [14]. $Atm^{-/-}$ NSCs showed a blunted response to environmental stress. They also display defective NSC proliferation and differentiation along a neuronal lineage, suggesting that ATM plays a role in adult neurogenesis [14]. Although substantial alterations of the subventricular zone (SVZ) tissues have been reported on several neurological disorders [15–17], alteration of the SVZ in A-T disease has remained unexplored. In the postnatal brain, once development is completed, the main role of the SVZ is to provide NSCs, which migrate toward the olfactory bulb for neuronal cell replacement and repair [16]. Otherwise NSCs in the SVZ are generally quiescent. Interestingly, recent studies of various animal models of neurodegeneration provide compelling evidence that NSCs can be activated to generate progenitor cells in response to stress or insults and then migrate to the sites to differentiate and replace the degenerated neurons [16–18]. For this reason, proper control of NSC self-renewal and differentiation is crucial for the maintenance of neural homeostasis and in determining the number of neuronal cells in the brain [18].

We have previously reported that in response to oxidative stress, p38 mitogen-activated protein kinase (hereafter called simply p38) is activated in $Atm^{-/-}$ NSCs; this activation is accompanied by reduced levels of the polycomb protein Bmi-1, which epigenetically controls the expression of p21. Reduction of Bmi-1 levels then results in defective proliferation of NSCs. However, treatment with a specific p38 inhibitor SB203580 restores normal levels of Bmi-1 and p21, as well as normal proliferation in cultured $Atm^{-/-}$ NSCs [19, 20]. In this study, we investigated whether results from our in vitro studies could be recapitulated in in vivo microenvironments of $Atm^{-/-}$ mice. In addition, we examined the feasibility of an in vivo therapeutic strategy by targeting oxidative stress-dependent p38 signaling in $Atm^{-/-}$ mice. Our data here showed that suppressing p38 activation by SB203580 not only restored $Atm^{-/-}$ NSCs but also increased the number of PCs in the cerebellum. More importantly, the motor coordination of $Atm^{-/-}$ mice was significantly improved. This study provides new insights into the therapeutic strategy for A-T and other neurodegenerative disorders by targeting specific signaling pathway in the resident NSCs.

## Materials and Methods

### Mice

The $Atm^{-/-}$ mice, originally developed by Barlow et al. [21], were purchased from the Jackson Laboratory (Bar Harbor, ME, http://www.jax.org). Offspring of $Atm^{+/-}$ breeders were genotyped using real-time polymerase chain reaction-based assays of tail DNA. *Atm* mice (1 month old) were divided into three groups: phosphate-buffered saline (PBS)-treated $Atm^{+/+}$ mice ($Atm^{+/+}$, $n = 10$ per group), PBS-treated $Atm^{-/-}$ mice ($Atm^{-/-}$, $n = 9$ per group), and SB203580-treated $Atm^{-/-}$ mice ($Atm^{-/-}$+SB, $n = 10$ per group). Mice were intraperitoneally injected with either PBS or SB203580 (5 mg/kg body weight) at 2-day intervals for 2 months. Animals were sacrificed 1 day after the last administration. Animal care was in accordance with the University of Texas M.D. Anderson Cancer Center guidelines for animal experiments.

### Histological Analysis of the SVZ and the Cerebellum by Immunofluorescence Staining

Mice were anesthetized and cardiac perfused through the heart with 4% paraformaldehyde. Brains were dissected out, post-fixed in the same fixative, and cryoprotected in 30% sucrose. Whole brains were frozen in Tissue-Tek optimal cutting temperature compound (O.C.T.) (VWR, Richmond, IL, http://www.vwr.com) and 7–12 $\mu$m coronal sections were collected at the level of anterior SVZ (1.0 to −0.5 mm bregma). Coronal cryostat sections were stained with hematoxylin/eosin (H&E) for cerebellar and for SVZ histology. Tissue sections were incubated in blocking solution consisting of 3% fetal bovine serum and 0.1% Triton X-100 (Sigma-Aldrich, St. Louis, http://www.sigmaaldrich.com) in PBS at room temperature for 30 minutes and then reacted with specific primary antibodies at 4°C overnight. Each sample was washed with PBS three times, for 10 minutes each, and then stained by secondary antibodies for 1 hour. Finally, each sample was sealed with mounting medium containing 4′,6-diamidino-2-phenylindole to stain cell nuclei and was visualized by fluorescence microscopy (Olympus IX2-SL; Olympus, Tokyo, http://www.olympus-global.com). Primary antibodies included nestin (Santa Cruz Biotechnology Inc., Santa Cruz, CA, http://www.scbt.com) and vimentin (Sigma-Aldrich) for the detection of undifferentiated neural progenitors, calbindin-D-28K (Sigma-Aldrich) for Purkinje cells, phospho-p38 (Cell Signaling Technology, Beverly, MA, http://www.cellsignal.com), Bmi-1 (Millipore, Billerica, MA, http://www.millipore.com), and p21 (Santa Cruz Biotechnology). Secondary antibodies included goat anti-mouse or anti-rabbit IgG and donkey anti-goat IgG (Jackson Immunoresearch Laboratories, West Grove, PA, http://www.jacksonimmuno.com) conjugated with a fluorescent dye (fluorescein isothiocyanate or Texas Red). Immunohistochemical slides were scanned using the Aperio ScanScope (Aperio, Vista, CA, http://www.aperio.com) through the Mutant Mouse Pathology Service at the M.D. Anderson Cancer Center.

### Quantification of Bromodeoxyuridine-Positive Cells

The total number of bromodeoxyuridine (BrdU)-positive cells in the SVZ was determined using unbiased stereological methods. Every fourth 12-$\mu$m coronal section throughout the lateral ventricle was examined and BrdU-positive cells within the SVZ were quantified, and the total number of BrdU-positive cells was then extrapolated by multiplying the number of cells counted by the reciprocal of the fraction of tissue that was quantified.

### Quantitative Reverse Transcription-Polymerase Chain Reaction

mRNA expression levels of *nestin*, *ki-67*, *bmi-1*, *p21$^{Cip1}$*, *Calbindin-K*, and *gfap* were quantified relative to *gapdh*, an internal RNA control, by quantitative reverse transcription-polymerase chain reaction (qRT-PCR). Primers were purchased from Sigma-Aldrich or Applied Biosystems (Foster City, CA, http://www.appliedbiosystems.com), and sequences are listed as follows. The primer that amplified *nestin* was Mm03053308_g1. The primer that amplified *ki-67* was Mm03053308_g1. The primer that amplified *bmi-1* was Mm03053308_g1. The primer that amplified *p21Cip1*: cdkn1a (p21) was Mm00432448_m1. Primer that amplified *Calbindin-K* were

sense, 5′-AGAATCCCACCTGCAGTCATCTC-3′, and antisense, 5′-TCCTTCCAGGTAACCACTTCCG-3′. Primers that amplified *gfap* were sense, 5′-AGAAACCAGCCTGGACACCAAATC-3′, and antisense, 5′-ACCACGATGTTCCTCTTGAGGTG-3′.

### Differentiation of Neural Stem Cells

Neurospheres were obtained from the SVZ of a postnatal day 1 (P1) pup and were maintained in culture essentially as reported [19]. The cells were seeded onto chamber slides and then maintained in medium containing 10% fetal bovine serum without epidermal growth factor for 7 days. Antibodies used for characterization of differentiated cells were anti-Map2 (Cell Signaling Technology) and anti-glial fibrillary acidic protein (GFAP) (Santa Cruz Biotechnology).

### Neuromotor Coordination Test

We have devised a new apparatus that combines walking across and balancing on a beam to test the motor coordination and equilibrium of the mice (supplemental online Figure 1). The beam (0.7 cm in diameter and 30 cm long) was spun at a speed of 25 rpm, controlled by a rotator. Prior to the test, $Atm^{+/+}$ and $Atm^{-/-}$ mice had training on the rotating beam with three trials per day for 3 days to sustain mice on a rotating beam. Following training, the motor coordination of the mouse was scored by measuring the time in seconds that the mouse stayed on the rotating beam before falling off. Three trials of mouse motor coordination were assessed.

### Statistical Analysis

For each experiment, data are presented as the mean ± SD of values. Each experiment was repeated at least three times. Statistical comparisons of values were made using an analysis of variance, followed by Bonferroni's post hoc test. Differences were considered significant when $p < .05$. Analyses of data were performed using Prism 5 Software (GraphPad Software, Inc., San Diego, http://www.graphpad.com).

## Results

### NSCs Are Decreased in the SVZ of $Atm^{-/-}$ Mice

To investigate whether results from in vitro culture [19, 20] are recapitulated in vivo in of $Atm^{-/-}$ mice, we examined SVZ cytoarchitecture of adult (P90) $Atm^{+/+}$ ($n = 4$) and $Atm^{-/-}$ mice ($n = 4$). The wall architecture of the lateral ventricle of $Atm^{-/-}$ mice was found to be normal. However, the NSC-selective marker nestin was significantly reduced by >90% loss in the SVZ of $Atm^{-/-}$ mice compared with $Atm^{+/+}$ controls (Fig. 1A, upper panels). The proliferation marker Ki67 was also significantly decreased in the same section of $Atm^{-/-}$ mice compared with that of $Atm^{+/+}$ mice (Fig. 1A, middle and lower panels). In accordance with this result, qRT-PCR analysis using total RNA purified from SVZ tissue also revealed that mRNA expressions of *nestin* and *Ki-67* in the SVZ of $Atm^{-/-}$ mice were reduced (Fig. 1B). To further confirm a decrease in proliferating cells in the SVZ region in vivo, BrdU was injected into adult mice (P90) for 5 days, and brains were examined. The number of BrdU-positive cells was counted within the SVZ. $Atm^{-/-}$ mice showed a decrease in BrdU-positive cells, especially apparent at the lateral segment of the lateral ventricle (Fig. 1C). This observation is consistent with our in vitro data of defective proliferation in $Atm^{-/-}$ NSCs [19, 20]. This is the first in vivo evidence showing that in the absence of ATM, the NSC population in the SVZ is decreased and exhibits decreased proliferation.

### Suppression of p38 Activation by SB203580 Restores NSCs in the SVZ of $Atm^{-/-}$ Mice

We previously reported that activation of p38 signaling in response to elevated ROS levels in $Atm^{-/-}$ NSCs resulted in defective self-renewal and proliferation in culture [19]. We therefore asked whether ATM deficiency alters the activation status of p38 in SVZ in vivo and whether altered p38 signaling may result in NSC reduction in the SVZ of $Atm^{-/-}$ mice. Immunofluorescence staining revealed increased levels of phospho-p38 in the SVZ of $Atm^{-/-}$ mice compared with in the SVZ of $Atm^{+/+}$ mice (Fig. 2A). This p38 activation was also evident in $Atm^{-/-}$ mice SVZ tissue by Western blot analysis using antibody against phospho-p38 (Fig. 2B). On the basis of these results, we hypothesized that treatment with pharmacologic inhibition of the p38 signaling should restore the NSC population in the SVZ of $Atm^{-/-}$ mice. In an attempt to test our hypothesis, we treated 1-month-old $Atm^{-/-}$ mice with p38 specific inhibitor SB203580 for 2 months and then compared the levels of nestin and Ki-67 in the SVZ with PBS-treated $Atm^{-/-}$ mice. We observed that both nestin and Ki-67 levels were significantly reduced in the SVZ of PBS-treated $Atm^{-/-}$ mice (hereafter called $Atm^{-/-}$ mice) compared with PBS-treated $Atm^{+/+}$controls ($Atm^{+/+}$) but improved in the SVZ of SB203580-treated $Atm^{-/-}$ mice ($Atm^{-/-}$+SB). However, SB203580 did not fully recover the levels of nestin and Ki-67 in the SVZ of $Atm^{-/-}$ mice, indicating that p38 activation may be only partially responsible for the NSC decrease in vivo (data not shown).

Next, we analyzed effects of the treatment on the NSC proliferation-promoting protein Bmi-1 and its downstream molecule p21 [19, 20], along with another NSC-selective marker, vimentin, in the SVZ. Immunofluorescence staining revealed that vimentin and Bmi-1 levels were reduced in the SVZ of $Atm^{-/-}$ mice compared with $Atm^{+/+}$mice, but SB203580 improved those levels in the SVZ of $Atm^{-/-}$ mice. We also observed that ATM deficiency resulted in an increase in p21 intensity and that SB203580 treatment decreased its level (Fig. 2C). In accordance with this result, Western blot analysis using the SVZ tissue further confirmed restoration effect by SB203580 (Fig. 2D). qRT-PCR analysis revealed that mRNA expression of *bmi-1* remained unaffected, although Bmi-1 protein levels in the SVZ of $Atm^{-/-}$ mice were greatly reduced. This result is consistent with our previous reported data that Bmi-1 expression level is regulated by a post-transcriptional mechanism in $Atm^{-/-}$ NSCs [20]. By contrast, *p21* mRNA expression was decreased by SB203580, confirming that inhibition of p38 restores Bmi-1 protein levels in the SVZ of $Atm^{-/-}$ mice, which suppresses expression of p21 (Fig. 2E). These data support the idea that p38 signaling suppresses NSC survival and proliferation through downregulation of Bmi-1 with the resultant upregulation of p21 in the SVZ of $Atm^{-/-}$ mice. However, these observations also indicate that p38 activation may not be completely responsible for the NSC decline and downregulation of Bmi-1 in the SVZ of $Atm^{-/-}$ mice in vivo.

### SB203580 Treatment Improves $Atm^{-/-}$ Cerebellar Purkinje Cells

ATM deficiency affects the cerebellum, leading to poor motor coordination in A-T patients [1, 3, 4]. We have also previously

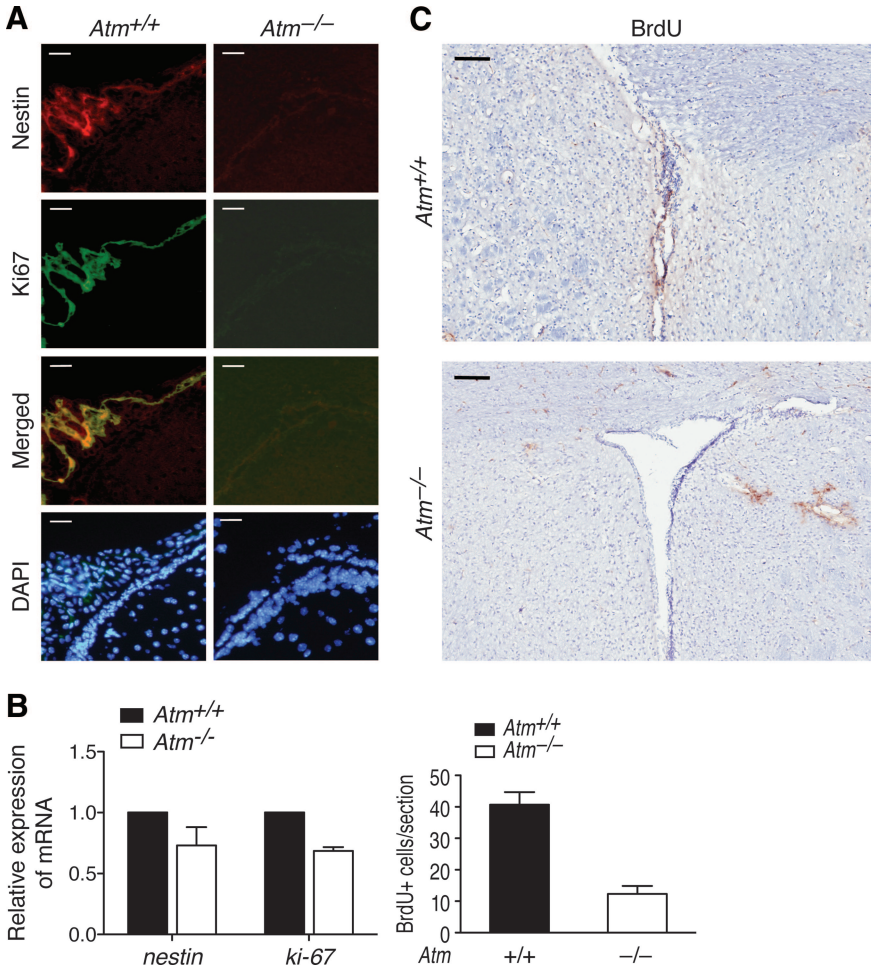


**Figure 1.** NSC depletion in the subventricular zone (SVZ) of $Atm^{-/-}$ mice. **(A):** Paraformaldehyde-fixed frozen sections of SVZ tissue of adult (postnatal day 90 [P90]) $Atm^{+/+}$ and $Atm^{-/-}$ mice were stained with antibodies against nestin (red) to identify NSCs and against Ki67 (green) to detect proliferating cells in the SVZ. Cells were counterstained by DAPI (blue), which identifies the nuclei of the NSCs. Scale bars = 50 $\mu$m. **(B):** Total RNA was purified from SVZ tissue of adult (P90) $Atm^{+/+}$ and $Atm^{-/-}$ mice and subjected to quantitative reverse transcription-polymerase chain reaction analysis for *nestin* and *Ki-67* mRNA expression. Probing for *gapdh* was used as an internal control. **(C):** After injection of adult (P90) $Atm^{+/+}$ and $Atm^{-/-}$ mice with BrdU for a period of 5 days, SVZ sections were stained with an antibody against BrdU to label proliferating cells. Scale bars = 100 $\mu$m. BrdU-positive cells in the SVZ of adult (P90) $Atm^{+/+}$ and $Atm^{-/-}$ mice were counted. Values represent BrdU-positive cell numbers in an SVZ section of $Atm^{+/+}$ mice ± SD (three independent countings of three sections). Abbreviations: BrdU, bromodeoxyuridine; DAPI, 4′,6-diamidino-2-phenylindole.

shown that degenerated PCs occur in the Purkinje cell layer (PCL) of the cerebellum of $Atm^{-/-}$ mice [6, 10]. Therefore, we investigated whether the cerebellum exhibits atrophy in $Atm^{-/-}$ mice and whether the protective effect of SB203580 influences cerebellar PCs in $Atm^{-/-}$ mice. We examined cerebella cytoarchitecture and the distribution and the number of the PCs in the PCL of cerebellum in 2- and 3-month-old $Atm^{+/+}$ and $Atm^{-/-}$ mice. PCs were stained with the selective protein marker calbindin. Cerebella in both 2-month-old $Atm^{+/+}$ and $Atm^{-/-}$ mice had a normal trilaminar architecture with intact molecular layer, PCL, and granule cell layers. In addition, no significant difference in distribution and the number of PCs along the PCL was observed between $Atm^{+/+}$ and $Atm^{-/-}$ mice (supplemental online Figure 2). This finding is consistent with a previous report by Barlow et al. showing that no obvious loss of cerebellar PCs is seen in the cerebellum of 2-month-old in $Atm^{-/-}$ mice [21]. However, 3-month-old $Atm^{-/-}$ cerebellum showed altered distribution of PCs in the PCL as compared with $Atm^{+/+}$ control (Fig. 3A). Immunostaining with calbindin antibody revealed that the number of PCs along the PCL decreased by 30% in $Atm^{-/-}$ mouse cerebellum compared with controls. Importantly, we also found that by 60 days after treatment, SB203580-treated $Atm^{-/-}$ mice displayed improved cytoarchitecture and more PCs along the PCL of the cerebellum (Fig. 3B, 3C). Analysis of calbindin protein and mRNA expression further confirmed PCs loss in $Atm^{-/-}$ cerebellum and restoration of those cells by SB203580 treatment (Fig. 3D, 3E).

On the basis of the observation that elevated levels of ROS occurs in $Atm^{-/-}$ mice brain [6, 22], our finding that p38 is activated in response to elevated ROS, and our data above showing that activation of p38 in the SVZ resulted in NSC loss in the SVZ of $Atm^{-/-}$ mice [19], we asked whether ATM deficiency also alters the activation status of p38 in the cerebellum and whether the reduced number of PCs is correlated to altered p38 signaling in the cerebellum of $Atm^{-/-}$ mice. Immunofluorescence staining revealed that phospho-p38 was found more intensively throughout PCs along the PCL of $Atm^{-/-}$ cerebellum; however, it was

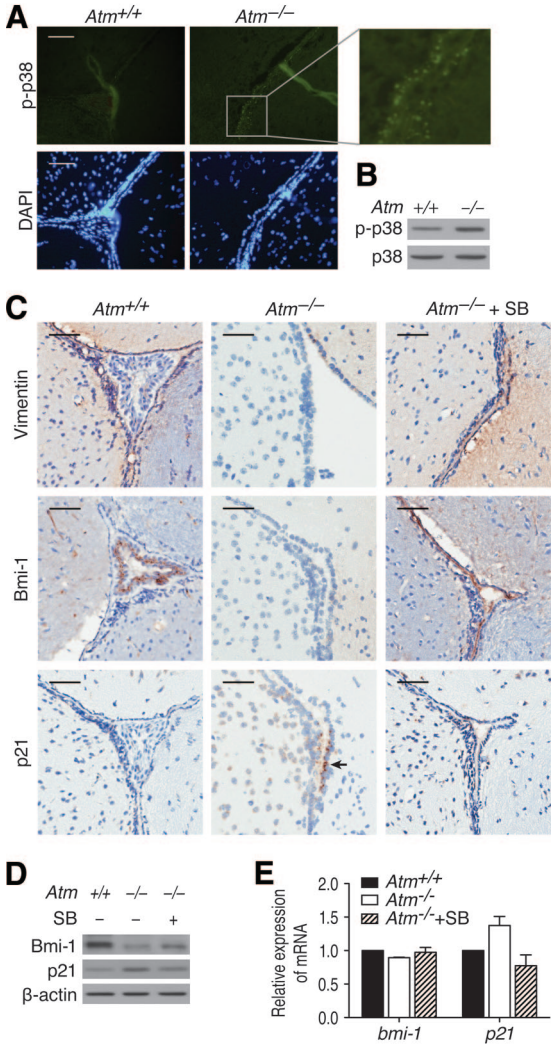


**Figure 2.** p38 activation is responsible for abnormalities in the subventricular zone (SVZ) of $Atm^{-/-}$ mice. **(A):** SVZ sections of adult (postnatal day 90 [P90]) $Atm^{+/+}$ and $Atm^{-/-}$ mice were stained with antibody against phospho-p38 (green). Cells were counterstained by DAPI. The right panel is an enlargement of the small gray framed area. Scale bars = 20 $\mu$m. **(B):** Proteins were extracted from SVZ tissue of adult (P90) $Atm^{+/+}$ and $Atm^{-/-}$ mice, and p38 activation was determined by Western blot analysis with an antibody against phospho-p38. **(C):** 1-month-old $Atm^{+/+}$ and $Atm^{-/-}$ mice were treated with either phosphate-buffered saline (PBS) or SB203580 for 2 months. $Atm^{+/+}$, $n = 10$; $Atm^{-/-}$, $n = 9$; $Atm^{-/-}$+SB, $n = 10$. After treatment, SVZ sections were stained with an antibody against another NSC-specific protein, vimentin, to identify NSCs. Sections were also stained with antibodies against Bmi-1 and p21. Arrow indicates p21-expressing cells. Scale bar = 50 $\mu$m. **(D):** Protein levels of Bmi-1 and p21 were determined by Western blot analysis using protein extracts from SVZ tissue of adult (P90) $Atm^{+/+}$, $Atm^{-/-}$, and $Atm^{-/-}$+SB mice. **(E):** Expression of *bmi-1* and *p21* mRNA was determined by quantitative reverse transcription-polymerase chain reaction using total RNA from SVZ tissue of adult (P90) $Atm^{+/+}$, $Atm^{-/-}$, and $Atm^{-/-}$+SB mice. Probing for *gapdh* was used as an internal control. Abbreviations: $Atm^{+/+}$, PBS-treated $Atm^{+/+}$; $Atm^{-/-}$, PBS-treated $Atm^{-/-}$; $Atm^{-/-}$+SB, SB203580-treated $Atm^{-/-}$; DAPI, 4′,6-diamidino-2-phenylindole; p-p38, phospho-p38; SB, SB203580.

only sparsely observed in $Atm^{+/+}$ cerebellum, but it was reduced again close to normal levels by SB203580 treatment in $Atm^{-/-}$ mice (data not shown). Our data demonstrate the p38 activation in $Atm^{-/-}$ cerebellum and suggest that restoration of

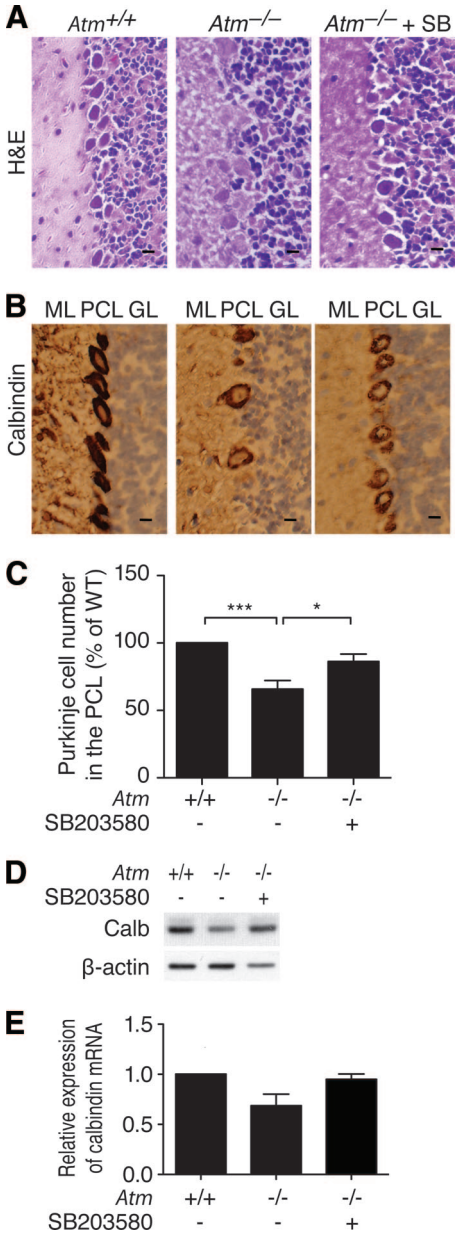


**Figure 3.** SB203580 protected $Atm^{-/-}$ cerebella Purkinje cells. **(A):** After treatment, cerebellum sections of adult (postnatal day 90 [P90]) $Atm^{+/+}$, $Atm^{-/-}$, and $Atm^{-/-}$+SB mice were stained with H&E to display cerebellum cytoarchitecture. **(B):** After treatment, cerebellum sections of adult (P90) $Atm^{+/+}$, $Atm^{-/-}$, and $Atm^{-/-}$+SB mice were stained with an antibody against calbindin to detect Purkinje cells. Scale bar = 20 $\mu$m. **(C):** Purkinje cell numbers along the PCL of cerebellar hemispheres of adult (P90) $Atm^{+/+}$, $Atm^{-/-}$, and $Atm^{-/-}$+SB mice were counted. Values represent percentage of $Atm^{+/+}$ Purkinje cell number ± SD (three independent counting of 10 fields; ***, $p < .001$; *, $p < .05$). **(D):** Protein levels of the Purkinje cell-specific protein calbindin were determined by Western blot analysis using protein extracts from cerebellar tissue of adult (P90) $Atm^{+/+}$, $Atm^{-/-}$, and $Atm^{-/-}$+SB mice. **(E):** Expression of *calbindin* mRNA was determined by quantitative reverse transcription-polymerase chain reaction using total RNA from cerebellar tissue of adult (P90) $Atm^{+/+}$, $Atm^{-/-}$, and $Atm^{-/-}$+SB mice. Probing for *gapdh* was used as an internal control. Abbreviations: $Atm^{+/+}$, PBS-treated $Atm^{+/+}$; $Atm^{-/-}$, PBS-treated $Atm^{-/-}$; $Atm^{-/-}$+SB, SB203580-treated $Atm^{-/-}$; Calb, calbindin; GL, granular layer; H&E, hematoxylin/eosin; ML, molecular layer; PCL, Purkinje cell layer; SB, SB203580; WT, wild-type.

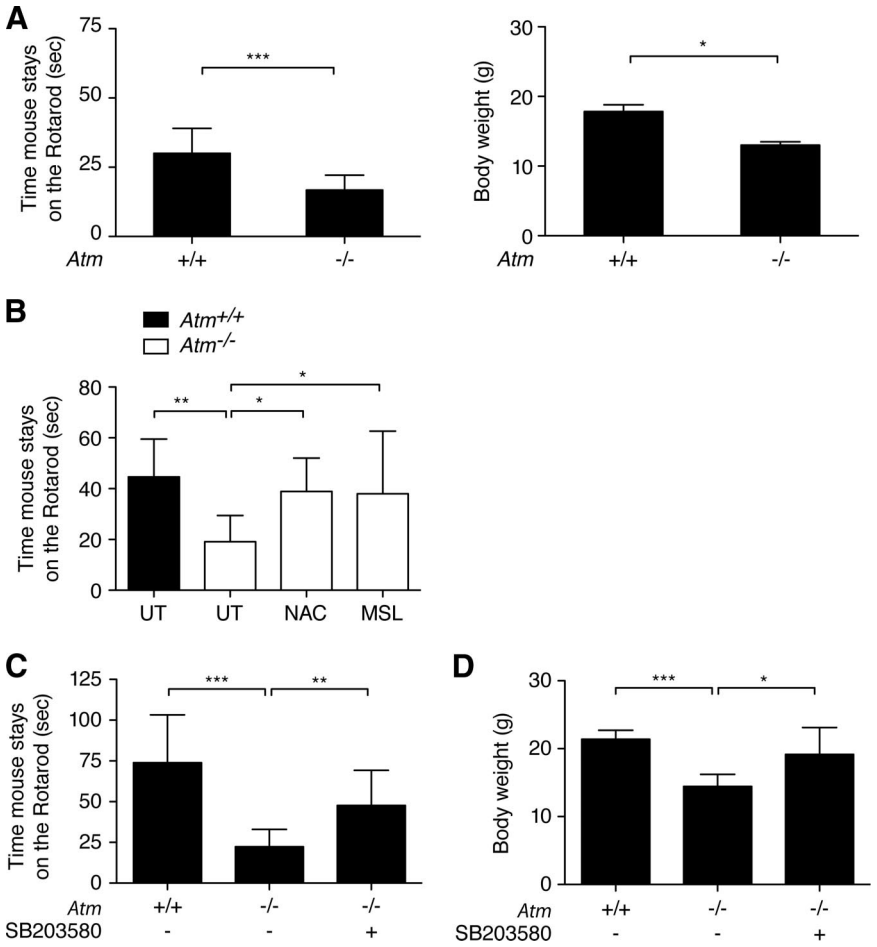


**Figure 4.** SB203580 retained the motor function of $Atm^{-/-}$ mice. **(A):** Motor coordination of 2-month-old $Atm^{+/+}$ and $Atm^{-/-}$ mice was analyzed by measuring the time before falling off the rotating beam at 25 rpm with three trials. Values represent means ± SD of time on the rotating rod ($Atm^{+/+}$, $n = 4$; $Atm^{-/-}$, $n = 4$; three independent tests; ***, $p < .001$). The body weights of 2-month-old $Atm^{+/+}$ and $Atm^{-/-}$ mice were also measured. Values represent means ± SD of body weights ($Atm^{+/+}$, $n = 4$; $Atm^{-/-}$, $n = 4$; three independent tests; *, $p < .05$). **(B):** After treatment with antioxidant NAC and MSL, motor coordination of adult (postnatal day 90 [P90]) $Atm^{+/+}$, $Atm^{-/-}$, $Atm^{-/-}$+NAC, and $Atm^{-/-}$+MSL mice were analyzed. Values represent means ± SD of time on the rotating beam ($n = 6$ per group; three independent tests; **, $p < .01$, *, $p < .05$). **(C):** After treatment, the motor coordination of adult (P90) $Atm^{+/+}$, $Atm^{-/-}$, and $Atm^{-/-}$+SB203580 (SB) mice was assessed by measuring the time before falling off the rotating beam at 25 rpm with three trials. Values represent means ± SD of time on the rotating beam ($Atm^{+/+}$, $n = 10$; $Atm^{-/-}$, $n = 9$; $Atm^{-/-}$+SB, $n = 10$; three independent tests; ***, $p < .001$, **, $p < .01$). **(D):** After treatment, the body weights of adult (P90) $Atm^{+/+}$, $Atm^{-/-}$, and $Atm^{-/-}$+SB mice were measured. Values represent means ± SD of body weights ($Atm^{+/+}$, $n = 10$; $Atm^{-/-}$, $n = 9$; $Atm^{-/-}$+SB, $n = 10$; three independent tests; ***, $p < .001$, *, $p < .05$). Abbreviations: MSL, monosodium luminol; NAC, *N*-acetyl-L-cysteine; UT, untreated.

the number of PCs in SB203580-treated mice may result from inhibiting p38 activation observed in $Atm^{-/-}$ cerebellum.

## SB203580 Treatment Recovers Motor Coordination of $Atm^{-/-}$ Mice

Although neuromotor deficits in $Atm^{-/-}$ mice do not reach the level of severity observed in A-T humans, histopathological evidence of altered SVZ and cerebellum is present in 3-month-old $Atm^{-/-}$ mice (Figs. 2, 3). The latter observation is consistent with our recent observations [10, 11]. In addition, the oxidative stress marker malondialdehyde was significantly increased in $Atm^{-/-}$ cerebellum compared with $Atm^{+/+}$ cerebellum [10]. The conventional rotarod test to prove neurological abnormalities in $Atm^{-/-}$ mice showed relatively small difference between $Atm^{+/+}$ and $Atm^{-/-}$ mice [21]. For more sensitive detection of the subtle differences, we have developed a new device with combination of beam traversal and the "falling off" test on a narrow beam to maximize motor performance difference (supplemental online Figure 1). This method is similar to that reported by our group recently [10]. Our modified motor coordination test outlined in methods allowed us to measure how long the mice can stay on the rotating beam and assess the functional recovery of motor coordination mediated by SB203580 treatment. Prior to the test, all mice had training of the rotarod test for 3 days, and they showed a stable learning of performance, as observed by an increase in the duration time on a beam. We found clear neuromotor and body weight differences between 2-month-old $Atm^{-/-}$ versus $Atm^{+/+}$ mice (Fig. 4A). Our protocol is a more sensitive test for the neuromotor coordination because $Atm^{-/-}$ mice showed a decrease of approximately 30%–40% in staying on the rotating beam in our protocol, but they show only a 10%–20% decrease in the conventional reported protocol [12]. To further substantiate our study, we proved that $Atm^{-/-}$ mice treated with antioxidant *N*-acetyl-L-cysteine and monosodium luminol (MSL) stayed on the beam as long as did $Atm^{+/+}$ mice

(Fig. 4B). These results are consistent with previous reports in antioxidant-treated $Atm^{-/-}$ mice [12, 13].

We then compared 3-month-old $Atm^{+/+}$ and $Atm^{-/-}$ mice with SB203580 treatment starting 1 month after birth. Throughout the study, $Atm^{+/+}$ mice consistently maintained balance on the rotarod for the mean latency of 75 seconds. Conversely, $Atm^{-/-}$ mice displayed significant motor impairment compared with $Atm^{+/+}$ control mice. This test disclosed a clear neuromotor coordination difference between $Atm^{+/+}$ and $Atm^{-/-}$ mice at 3 months of age, indicating that $Atm^{-/-}$ mice develop a movement disorder similar to ataxia in A-T humans. On the other hand, SB203580-treated mice performed significantly better on the beam than did the $Atm^{-/-}$ groups, although they did not fully perform similar to the levels of the $Atm^{+/+}$ mice group (Fig. 4C). Body weight measurements following the neuromotor coordination test showed that $Atm^{-/-}$ mice displayed significant weight loss compared with the $Atm^{+/+}$ mice, but SB203580-treated $Atm^{-/-}$ mice improved their body weights close to normal (Fig. 4D). In contrast, $Atm^{+/+}$ mice treated with SB203580 did not differ from their PBS-treated control group (data not shown), demonstrating no stressful nature of treatment. Taken together, our data suggest that SB203580 treatment has therapeutic effects that correct neuromotor deficits in $Atm^{-/-}$ mice.

## Discussion

During adult neurogenesis, NSCs in the SVZ are thought to functionally contribute to brain plasticity and repair because of their capacity for self-renewal and multipotency [18, 23]. Thus, elucidating the signaling pathways that control NSC self-renewal, proliferation, and differentiation may have important implications for treatment of neurodegenerative diseases. Once these pathways are identified, new avenues for research targeting NSCs will be opened, and appropriate strategies could be developed for regenerative medicine.

We previously reported that in response to ROS elevation, a p38-specific pathway plays a critical role in controlling the proliferation of NSCs [19, 20]. Here we verify this pathway in the SVZ of $Atm^{-/-}$ mice in vivo. At the neuropathological levels, we show that depletion of NSCs in the SVZ is a prominent feature in 3-month-old $Atm^{-/-}$ mice. In addition, levels of Bmi-1 are markedly lower in the SVZ of $Atm^{-/-}$ mice, compared with $Atm^{+/+}$ mice. Bmi-1, a component of the polycomb repressive complex, is necessary for normal NSC self-renewal and proliferation because it epigenetically silences genes that encode the cell cycle inhibitors p16, p19, and p21 [24–27]. Interestingly, regulation of p21 expression by Bmi-1 appears to be specific to NSCs [19], whereas Bmi-1 regulates p16 in response to oxidative stress in astrocytes and hematopoietic stem cells [28, 29]. Knockdown of *Bmi-1* results in upregulation of p21, which in turn, causes suppression of NSC self-renewal and proliferation [27]. This is in accordance with our observation here that higher levels of p21 also occur in the SVZ in $Atm^{-/-}$ mice in this study.

In spite of substantial alterations in the SVZ tissues in 3-month-old $Atm^{-/-}$ mice, no significant differences in dentate gyrus (DG) NSCs of the hippocampus were observed in our study (data not shown). However, it was previously reported that DG NSCs of $Atm^{-/-}$ mice exhibit an increase in proliferation between 41 and 44 days of age but show a decrease in survival between 68 and 71 days of age [14]. This discrepancy could be due to age difference between the mice examined or due to age and functional differences between DG NSCs and SVZ NSCs. The subgranular zone of the DG is one of the main regions known to have high rates of neurogenesis because of its primary function in memory formation [30]. The abnormal increase in proliferation at younger age could be a reflection of the DG NSCs, which reside in a proliferative environment. This increase in proliferation, however, with time leads to genomic instability, a precursor to loss of survival. A similar increase in proliferation in response to ROS has been reported in thymocytes and hematopoietic stem cells from young $Atm^{-/-}$ mice [29, 31].

We observed no obvious degeneration of PCs in 2-month-old $Atm^{-/-}$ mice, although we began to see a difference in coordination relative to $Atm^{+/+}$ mice. These observations are consistent with previous reports that 2-month-old $Atm^{-/-}$ mice show considerable variation from barely detectable to moderate changes in cerebellar degeneration, but they exhibit neurobehavioral deficits [5, 7–11]. However, by 3 months of age, we observe visible cerebellar degeneration, which is accompanied by marked increased motor coordination deficits, a phenotype similar to that seen in A-T patients [3, 4]. Together our data indicate that motor coordination deficit, due to dysfunctional neurons such as defects in synapses, could occur before visible neurodegeneration. Once neurons die, the only way we can replace them is by stem cell therapy and if possible by targeting the brain's own NSCs. Therefore, this observation may offer some hope in A-T therapy because it is still possible to slow down the degenerative process and rescue the neurons from demise at a time when we observe clinical signs of motor coordination deficits.

We show that p38 inhibition restores NSCs within the SVZ and has beneficial effects in the cerebellum of the $Atm^{-/-}$ mice, as well as correcting their motor incoordination. In addition to its p38-specific inhibitory effect, SB203580, a sulfonyl imidazole, can also act as a redox buffer, which could correct the redox stress. However, the specific inhibitory effect of SB203580 on p38 and its antioxidant effects are not necessarily mutually exclusive [19]. Our data here demonstrate p38 activation in the SVZ and PCs in the cerebellum of $Atm^{-/-}$ mice, suggesting that both the SVZ and cerebellar PCs are affected by the constitutive oxidative stress in ATM deficiency. Thus, ATM deficiency has global effects on all cell types, albeit some may be more vulnerable to oxidative stress than others. Our findings substantiate the notion that oxidative stress is the primary culprit causing neurological deficits in $Atm^{-/-}$ mice. In this regard, we recently showed that a potent redox buffering agent, MSL, alleviates redox stress and restores the motor coordination deficits in $Atm^{-/-}$ mice [10]. As for the role of ROS-mediated p38 activation in neurodegeneration, other researchers have shown that in response to ROS, p38 is activated in human Alzheimer's disease and in an Alzheimer's mouse model. In this mouse model, p38 inhibitor also restored the brain abnormality [32]. Therefore, ROS and p38 signaling in the brain are potential targets for A-T neurodegeneration.

It remains unclear whether functionally enriched SVZ NSCs by a p38 inhibitor bring a beneficial consequence to PCs in the cerebellum and attenuate neuromotor deficits in $Atm^{-/-}$ mice. NSCs in the SVZ normally migrate to the olfactory bulb. However, studies on mouse models of Parkinson's, Huntington's,

and Alzheimer's diseases have indicated that NSCs could be activated and migrate to the site of damage [33]. Normal p38 signaling is essential for neuronal differentiation [34], and p38 activation resulted in abnormal differentiation in $NPC1^{-/-}$ NSCs [35]. By contrast, p38 signaling is suppressed in proliferating NSCs [36]. Here we observed that p38 signaling was activated in the SVZ of $Atm^{-/-}$ mice, which contributed to a decrease in NSCs. We also showed that $Atm^{-/-}$ NSCs derived from the SVZ were capable of undergoing differentiation, but they had different frequencies of differentiation into cells of the neural lineage compared with $Atm^{+/+}$ NSCs, evidenced by different compositions of differentiated GFAP-positive astrocytes and Map2-positive neurons (supplemental online Figure 3). It is possible that the SVZ of $Atm^{-/-}$ mice is depleted in proliferating NSCs but enriched in the quiescent NSCs, which still maintain the ability to differentiate, albeit abnormally. It is possible that p38 inhibition could enhance migration of NSCs to damaged cerebellum tissue in the $Atm^{-/-}$ mice and shift the differentiation fate of their progeny to replenish the degenerated neurons. To prove this speculation, it would be very important to show that the NSCs in the SVZ indeed migrate to the cerebellum to replenish damaged PCs in the $Atm^{-/-}$ mouse brain. We realize that this kind of study in the brain is very difficult, and further intensive studies to address this question are warranted.

## Conclusion

Here we show that the $Atm^{-/-}$ mice used for the present study recapitulate neuropathological phenotypes of A-T patients as a useful model to elucidate the mechanisms underlying neurodegeneration and to test strategies for the treatment of A-T disease. We demonstrate that the SVZ region of $Atm^{-/-}$ mouse has intrinsic impairments in NSC survival that may lead to abnormal differentiation. Importantly, we identified that the p38 signaling pathway in the NSCs can be modulated by small molecule to rescue the ROS-mediated neurological defects in $Atm^{-/-}$ mouse. We believe that controlling NSC function and survival may be therapeutically useful in the treatment of A-T neurodegeneration. Although we realize that targeting NSCs in situ is a promising approach for regenerative medicine, it is just the first step on a long road to translate this approach to human translational medicine. More knowledge is required and many obstacles must be overcome before this can become a genuine therapeutic option for the treatment of A-T and other neurodegenerative diseases.

## Acknowledgments

We are grateful to Lifang Zhang for injection of SB203580 to mice. This project was supported with funding from the Longevity Foundation (formerly, the A-T Foundation) (Texas, U.S.) and Action for A-T (U.K.).

## Author Contributions

J.K.: conception and design, provision of study material or patients, data analysis and interpretation, manuscript writing; P.K.Y.W.: conception and design, financial support, administrative support, data analysis and interpretation, manuscript writing, final approval of manuscript.

## Disclosure of Potential Conflicts of Interest

The authors indicate no potential conflicts of interest.

## References

**1** Gatti RA, Boder E, Vinters HV et al. Ataxia-telangiectasia: An interdisciplinary approach to pathogenesis. Medicine (Baltimore) 1991; 70:99–117.

**2** Wong PKY, Kim J, Kim SJ et al. Oxidative stress-mediated neurodegeneration: A tale of two models. In: McNeil AS, ed. Neurodegeneration: Theory, Disorders and Treatments. Nova Science Publishers, Inc. 2010:1–44.

**3** Paula-Barbosa MM, Ruela C, Tavares MA et al. Cerebellar cortex ultrastructure in ataxia-telangiectasia. Ann Neurol 1983;13:297–302.

**4** Bottini AR, Gatti RA, Wirenfeldt M et al. Heterotopic Purkinje cells in ataxia-telangiectasia. Neuropathology 2012;32:23–29.

**5** Kuljis RO, Xu Y, Aguila MC et al. Degeneration of neurons, synapses, and neuropil and glial activation in a murine $Atm^{-/-}$ model of ataxia-telangiectasia. Proc Natl Acad Sci USA 1997;94:12688–12693.

**6** Liu N, Stoica G, Yan M et al. ATM deficiency induces oxidative stress and endoplasmic reticulum stress in astrocytes. Lab Invest 2005;85:1471–1480.

**7** Eilam R, Peter Y, Elson A et al. Selective loss of dopaminergic nigro-striatal neurons in brains of Atm-deficient mice. Proc Natl Acad Sci USA 1998;95:12653–12656.

**8** Eilam R, Peter Y, Groner Y et al. Late degeneration of nigro-striatal neurons in ATM−/− mice. Neuroscience 2003;121:83–98.

**9** Borghesani PR, Alt FW, Bottaro A et al. Abnormal development of Purkinje cells and lymphocytes in Atm mutant mice. Proc Natl Acad Sci USA 2000;97:3336–3341.

**10** Kuang X, Yan M, Ajmo JM et al. Activation of AMP-activated protein kinase in cerebella of Atm−/− mice is attributable to accumulation of reactive oxygen species. Biochem Biophys Res Commun 2012;418:267–272.

**11** Li J, Chen J, Ricupero CL et al. Nuclear accumulation of HDAC4 in ATM deficiency promotes neurodegeneration in ataxia telangiectasia. Nat Med 2012 [Epub ahead of print].

**12** Browne SE, Roberts LJ 2nd, Dennery PA et al. Treatment with a catalytic antioxidant corrects the neurobehavioral defect in ataxia-telangiectasia mice. Free Radic Biol Med 2004; 36:938–942.

**13** Gueven N, Luff J, Peng C et al. Dramatic extension of tumor latency and correction of neurobehavioral phenotype in Atm-mutant mice with a nitroxide antioxidant. Free Radic Biol Med 2006;41:992–1000.

**14** Allen DM, van Praag H, Ray J et al. Ataxia telangiectasia mutated is essential during adult neurogenesis. Genes Dev 2001;15:554–566.

**15** Quiñones-Hinojosa A, Chaichana K. The human subventricular zone: A source of new cells and a potential source of brain tumors. Exp Neurol 2007;205:313–324.

**16** Curtis MA, Faull RL, Eriksson PS. The effect of neurodegenerative diseases on the subventricular zone. Nat Rev Neurosci 2007;8: 712–723.

**17** Oizumi H, Hayashita-Kinoh H, Hayakawa H et al. Alteration in the differentiation-related molecular expression in the subventricular zone in a mouse model of Parkinson's disease. Neurosci Res 2008;60:15–21.

**18** Gage FH. Mammalian neural stem cells. Science 2000;287:1433–1438.

**19** Kim J, Wong PK. Loss of ATM impairs proliferation of neural stem cells through oxidative stress-mediated p38 MAPK signaling. Stem Cells 2009;27:1987–1998.

**20** Kim J, Hwangbo J, Wong PK. p38 MAPK-mediated Bmi-1 down-regulation and defective proliferation in ATM-deficient neural stem cells can be restored by Akt activation. PLoS One 2011;6:e16615.

**21** Barlow C, Hirotsune S, Paylor R et al. Atm-deficient mice: A paradigm of ataxia telangiectasia. Cell 1996;86:159–171.

**22** Barlow C, Dennery PA, Shigenaga MK et al. Loss of the ataxia-telangiectasia gene product causes oxidative damage in target organs. Proc Natl Acad Sci USA 1999;96:9915–9919.

**23** Deng W. Neurobiology of injury to the developing brain. Nat Rev Neurol 2010;6:328–336.

**24** Molofsky AV, He S, Bydon M et al. Bmi-1 promotes neural stem cell self-renewal and

neural development but not mouse growth and survival by repressing the p16Ink4a and p19Arf senescence pathways. Genes Dev 2005; 19:1432–1437.

**25** Molofsky AV, Pardal R, Iwashita T et al. Bmi-1 dependence distinguishes neural stem cell self-renewal from progenitor proliferation. Nature 2003;425:962-967.

**26** Leung C, Lingbeek M, Shakhova O et al. Bmi1 is essential for cerebellar development and is overexpressed in human medulloblastomas. Nature 2004;428:337–341.

**27** Fasano CA, Dimos JT, Ivanova NB et al. shRNA knockdown of Bmi-1 reveals a critical role for p21-Rb pathway in NSC self-renewal during development. Cell Stem Cell 2007;1:87–99.

**28** Kim J, Wong PK. Oxidative stress is linked to ERK1/2-p16 signaling-mediated growth defect in ATM-deficient astrocytes. J Biol Chem 2009;284:14396–14404.

**29** Ito K, Hirao A, Arai F et al. Reactive oxygen species act through p38 MAPK to limit the lifespan of hematopoietic stem cells. Nat Med 2006;12:446–451.

**30** Saab BJ, Georgiou J, Nath A et al. NCS-1 in the dentate gyrus promotes exploration, synaptic plasticity, and rapid acquisition of spatial memory. Neuron 2009;63:643–656.

**31** Yan M, Qiang W, Liu N et al. The ataxia-telangiectasia gene product may modulate DNA turnover and control cell fate by regulating cellular redox in lymphocytes. FASEB J 2001;15:1132–1138.

**32** Munoz L, Ralay Ranaivo H, Roy SM et al. A novel p38 alpha MAPK inhibitor suppresses brain proinflammatory cytokine up-regulation and attenuates synaptic dysfunction and behavioral deficits in an Alzheimer's disease mouse model. J Neuroinflammation 2007;4: 21.

**33** Leong SY, Faux CH, Turbic A et al. The Rho kinase pathway regulates mouse adult neural precursor cell migration. Stem Cells 2011;29: 332–343.

**34** Androutsellis-Theotokis A, Leker RR, Soldner F et al. Notch signaling regulates stem cell numbers in vitro and in vivo. Nature 2006; 442:823–826.

**35** Yang SR, Kim SJ, Byun KH et al. NPC1 gene deficiency leads to lack of neural stem cell self-renewal and abnormal differentiation through activation of p38 mitogen-activated protein kinase signaling. Stem Cells 2006;24:292–298.

**36** Lim MS, Nam SH, Kim SJ et al. Signaling pathways of the early differentiation of neural stem cells by neurotrophin-3. Biochem Biophys Res Commun 2007;357:903–909.

See www.StemCellsTM.com for supporting information available online.

# Targeting p38 Mitogen-Activated Protein Kinase Signaling Restores Subventricular Zone Neural Stem Cells and Corrects Neuromotor Deficits in *Atm* Knockout Mouse

Jeesun Kim and Paul K.Y. Wong

*Stem Cells Trans Med* published online July 6, 2012